JOURNAL OF MATERIALS SCIENCE **39** (2004) 7303–7316

Oxidation mechanisms and kinetics of SiC-matrix composites and their constituents

R. NASLAIN, A. GUETTE, F. REBILLAT, S. LE GALLET, F. LAMOUROUX, L. FILIPUZZI, C. LOUCHET
Laboratory for Thermostructural Composites, UMR-5801 (CNRS, Snecma, CEA, UB1), University Bordeaux 1, 3 Allée de La Boetie, 33600 Pessac, France

The oxidation kinetics and mechanisms of SiC-matrix composites fabricated by chemical vapor infiltration, and of their constituents (C or SiC-fibers, C or BN interphases and SiC matrix) are studied on the basis of an experimental approach and modelling. The oxidation of carbon fibers is rate-controlled by a combined diffusion/chemical reaction mechanism at low temperatures and its rate reduced by a 1600°C heat treatment. The oxidation rate of the pyrocarbon is similar to that of the fibers when they have been heat-treated. The oxidation kinetics of both the SiC-based fibers and matrix are parabolic and assumed to be rate-limited by the diffusion of gaseous species in the silica scale. A full kinetics law is given. The occurrence of water in the atmosphere increases the oxidation rate of the fibers and decreases the activation energy, water becoming the main oxidizing agent. The oxidation of the BN-interphase is complex and strongly anisotropic, its kinetics depending on composition, structure and texture. Finally, the oxidation of SiC-matrix composites, depicted for 1D-SiC/C/SiC and 2D-C/C/SiC composites, involves both diffusion of gaseous species in the composite porosity and heterogeneous oxidation reactions. Oxidation occurs through the thickness of the composites at low temperatures which consumes the carbon-based constituents. Conversely, it tends to be limited to near the composite surface at high temperatures, due to the formation of silica-based phases healing the material porosity and preventing the in-depth oxidation of the carbon-based constituents.

1. Introduction

SiC-based composites usually consist of carbon or SiC fibers embedded in a SiC-matrix. They display the outstanding property of being non-brittle when the fiber/matrix (FM) bonding is optimized (that is not too strong but not too weak) through the use of a thin layer of a compliant material referred to as the *interphase* which is deposited on the fiber surface before the infiltration of the SiC-matrix [1]. The most commonly used interphase materials are pyrocarbon, i.e., a graphitic carbon deposited from a gaseous precursor, or hexagonal boron nitride, both exhibiting a layered crystal structure in which the layers (deposited parallel to the fiber surface) are weakly bonded to one another. The main role of the interphase is to arrest and/or deflect the microcracks which are formed under load in the brittle SiC-matrix, avoiding thus the early failure of the brittle fibers by a notch effect. Hence, the interphase protects the load-bearing fibers and is sometimes referred to as a *mechanical fuse* [2].

SiC-matrix composites being refractory, stiff and tough materials, are potential candidates for structural application at high temperatures, including in aerojet engines, rocket engines, gas turbines of cogeneration and first wall of nuclear fusion reactors [3]. In most cases, these materials are exposed for long periods of time (several 10,000 h in gas turbines) to the combined effect of temperature and load, in atmospheres which are frequently oxidizing. Since the different constituents of the materials are non-oxide ceramics, which are intrinsically oxidation-prone, a good knowledge of the oxidation mechanisms and kinetics of the composites and of their constituents is necessary to understand and model the behavior of the composites when exposed to severe service conditions [4–7].

The aim of the present contribution was to assess the oxidation mechanisms and kinetics of SiC-matrix composites and their constituents (fibers, interphase and matrix) through experiments usually performed on model substrates in the so-called passive oxidation regime and through modelling.

2. Experimental

2.1. Materials

Oxidation tests were performed on the following materials: (i) fibers commonly used in ceramic matrix composites (CMCs), namely, carbon and SiC-based ceramic fibers, (ii) SiC-matrix of SiC (fiber)/SiC composites, (iii) pyrocarbon and BN interphases and (iv) model unidirectional SiC (fiber)/SiC composites and real C (fiber)/SiC composites.

Three kinds of fibers have been used. The *carbon fibers* were T 300 high strength fibers (from Toray) produced by pyrolysis of a polyacrylonitrile (PAN) precursor at moderate temperature and which contain some residual nitrogen. They were used either as-received or after a thermal treatment (HTT, for high temperature treatment) performed at 1600°C, in order to stabilize their microstructure [5]. The SiC-*based fibers* were from two of the three fiber families commonly used as reinforcements in CMC, namely: (i) nanocrystalline Si–C–O fibers (Nicalon NLM 202, ceramic grade (CG) from Nippon Carbon, Japan) consisting of SiC nanocrystals and carbon clusters dispersed in an amorphous SiC_xO_y phase [8] and (ii) SiC + C oxygen-free fibers (Hi-Nicalon, also from Nippon Carbon) which consist of a mixture of SiC-nanocrystals and free carbon [9]. Their overall chemical composition was respectively: 57Si-32C-12O-0.06H (in wt%) corresponding to a C/Si at. ratio of 1.31, for the former, and 62Si-37C-0.5O (wt%) and C/Si (at) ≈ 1.39, for the latter. It is worthy of note that the fibers of the third family, referred to as quasi-stoichiometric SiC fibers (such as Hi-Nicalon type S, from Nippon Carbon) were not available when the present study was initiated and are the subject of a forthcoming study. The SiC-based fibers were desized before being submitted to the oxidation tests, according to conventional procedures (solvent extraction and/or oxidation in air at low temperature).

The pyrocarbon (PyC) and boron nitride *interphases* were deposited from a hydrocarbon (C_xH_y, usually methane) and $BX_3 + NH_3$ mixture gaseous precursors respectively, at a temperature of 900–1100°C and under reduced pressures, on different substrates including fibers (Nicalon or Hi-Nicalon) and flat model substrates (sintered SiC pellets), according to the following overall equations [6, 10, 12]:

$$2C_xH_{y(g)} \rightarrow 2xC_{(s)} + yH_{2(g)} \quad (1)$$

$$BX_3 + NH_{3(g)} \xrightarrow{(H_2 \text{or} Ar)} BN_{(s)} + 3HX_{(g)} \quad \text{with } X = F, Cl \quad (2)$$

The BN-deposits were first out-gased at 1000°C in the CVD reactor then heat treated, after having seen the ambient atmosphere (with some oxygen absorption), at the highest temperature compatible with the thermal stability of the fibers, in order to improve their state of crystallization (BN, deposited from $BCl_3 + NH_3$ precursor at low temperature, being known to be poorly crystallized and sensitive to moisture) [6].

The oxidation kinetics of the SiC-*matrix* were assessed through tests performed on the matrix of SiC/SiC composites prepared by the chemical vapor infiltration (CVI) process [10]. The SiC-matrix was deposited from a flowing gaseous mixture of methyltrichlorosilane (MTS) and hydrogen, at relatively low temperature (900–1100°C) and under reduced pressure (to favor the in-depth deposition), according to the following overall equation [10, 13]:

$$CH_3SiCl_{3(g)} \xrightarrow{(H_2)} SiC_{(s)} + 3HCl_{(g)} \quad (3)$$

It consisted mainly of β-SiC (cubic 3C-polytype) with a trace amount of free silicon. It was first formed within the open porosity of the fiber preform (infiltration or in-depth deposition) and then on its external surface (when the preform porosity became sealed by the deposit) as an over-coating (or seal-coat) of ≈120–150 μm. The oxidation test samples were cut from the composite with a diamond saw, as 3 × 3 × 3 mm^3 cubes, and their 150 μm SiC over-coating face polished with diamond pastes, according to conventional metallographic procedures for ceramics [4].

Finally, overall oxidation tests were performed on SiC-*matrix model and real composites*, in order to study the combined effect of the oxidation of their constituents. The model materials were unidirectional (1D) composites fabricated from one single fiber tow comprising several hundreds or thousands elementary filaments and usually referred to as minicomposites. The fibrous reinforcements were maintained straight during the successive deposition of the interphase (PyC or BN) and matrix with a ceramic holder, according to a technique which has been depicted elsewhere [14]. The real composites were fabricated from a bidirectional (2D) fiber preform consisting of a stack of woven carbon fabrics maintained pressed together with a graphite fixture during the infiltration of the interphase and matrix, by the isothermal/isobaric CVI process [10]. The SiC-matrix was deposited from the MTS + H_2 precursor, as described above. It was found close to stoichiometry and mainly consisted of β-SiC nanocrystals with a preferred orientation (their [111] direction being perpendicular to the fiber surface).

2.2. Oxidation tests

Most oxidation tests were performed with a thermogravimetric analysis (TGA) equipment (24 S 16 TGA apparatus, from SETARAM, France), at atmospheric pressure ($P \approx 100$ kPa) and in a flowing atmosphere consisting of either dry oxygen or dry oxygen-nitrogen mixtures. However, some experiments were conducted with oxygen-water vapor–nitrogen mixtures (with different partial pressures of either oxygen or water), with a modified TGA-apparatus (also from SETARAM) which has been described elsewhere [15]. The oxidation kinetics were mostly assessed from the variations of relative sample weight ($\Delta_m/m_o = 100\,(m - m_o)/m_o$, where m_o is the sample mass at $t = 0$ and m that at t) versus time curves. In a few cases, they were derived from the variations of the thickness X of material consumed (BN interphase) or that of the oxide scale (SiO_2) resulting from the oxidation process, as a function of time. This layer thickness was either directly measured by scanning electron microscopy or spectroreflectometry (Nanospec/AST-201), for silica scales [4] or calculated from TGA-curves according to models given elsewhere [6], for the oxidation of BN-interphases. Kinetics constants were calculated from the experimental kinetics curves and their variations as a function of temperature (Arrhenius plots) and oxygen (or water vapor) partial pressure established, when enough data could be collected, in order to derive apparent activa-

tion energies and apparent reaction orders, and finally to establish apparent kinetics laws that could be further utilized in modelling.

3. Results and discussion

3.1. Oxidation of carbon fibers and interphases

Isothermal oxidation tests were conducted in flowing oxygen on T 300 carbon fiber tows used either as-received, or after heat treatment (HTT = 1600°C) or coated with a pyrocarbon interphase deposited from methane. Oxidation of the fibers occurs with a weight loss corresponding to the formation of CO_2 and/or CO. The kinetics curves exhibit a classical sigmoidal shape, the oxidation rate first increasing (for $0 < \Delta m/m_o < 20\%$) then remaining almost constant for $20 < \Delta m/m_o < 70\%$ and finally decreasing (for $70 < \Delta m/m_o < 100\%$), as a function of time (Fig. 1a). The oxidation rate was almost constant within the second domain, with the kinetic constant k defined as:

$$k = -\frac{1}{m_o}\frac{dm}{dt} \tag{4}$$

and calculated for $\Delta m/m_o = 50\%$ in the following. As shown in Fig. 1b, its temperature dependence obeys an Arrhenius-type law within two temperature domains that will be referred to as the high and low temperature domains, respectively [5, 16]:

$$k = k_o \exp(-E_a/RT) \tag{5}$$

where k_o is a pre-exponential term, E_a the apparent activation energy, R the perfect gas constant and T the temperature in Kelvin. The data suggest the occurrence of two different oxidation mechanisms with $E_a = 80$ kJ/mol at low temperatures and $E_a = 15$ kJ/mol at high temperatures. It is worthy of note that the former is significantly increased (to $E_a = 150$ kJ/mol) when the fibers have been heat treated before the oxidation tests.

Generally speaking, the oxidation of a porous carbon (as a matter of fact, a carbon fiber tow displays both intrafiber nanoporosity and interfiber microporosity) involves *diffusion phenomena* (of the reactant and product) in the boundary stagnant gas layer surrounding the solid, corresponding to low E_a-values, on the one hand, as well as *surface chemical reactions* between carbon and gaseous species adsorbed on the so-called active sites (edges and in in-plane defects of the carbon layers) and related to much higher E_a-values, on the other hand [17, 18]. The low E_a-value ($E_a = 15$ kJ/mol), calculated for $750 < T < 950$°C, strongly suggests that the rate limiting phenomenon is the diffusion of the gaseous species (reactant or product) in the boundary layer. By contrast, the E_a-value calculated for $500 < T < 700$°C, namely 80 kJ/mol, is too low to be assigned to a pure rate control by the oxygen-carbon surface reaction (reported to be 160–200 kJ/mol). Tentatively, it is proposed that the oxidation of T 300 carbon fiber tow is rate controlled by a mixed in-pore diffusion/surface reaction mode, in the low temperature domain. This assumption is mainly based on the fact that these fibers are known to display a significant nanoporosity and poor structural organization in the as-produced state [5, 16]. However, the influence of catalytic impurities (such as alkali metal compounds) known to be present in carbon fibers prepared from PAN-precursor, cannot be ruled out.

Interestingly and as apparent from Fig. 1b, annealing the fibers at 1600°C does not change the oxidation mechanism at 800–900°C (diffusion rate control). Conversely, it reduces significantly the oxidation rate at low temperatures with an increase of the apparent activation energy (from 80 to 150 kJ/mol). E_a is now closer to that reported above for the oxygen-carbon surface chemical reaction but still lower than those reported for carbon fibers which have been prepared from mesophase precursors or/and treated at very high temperature and are partly graphitized ($E_a = 185$–195 kJ/mol). To conclude, the high oxidation rate observed at low temperatures for the as-received T 300 fibers is related to its poor overall structural organization (and possibly to the occurrence

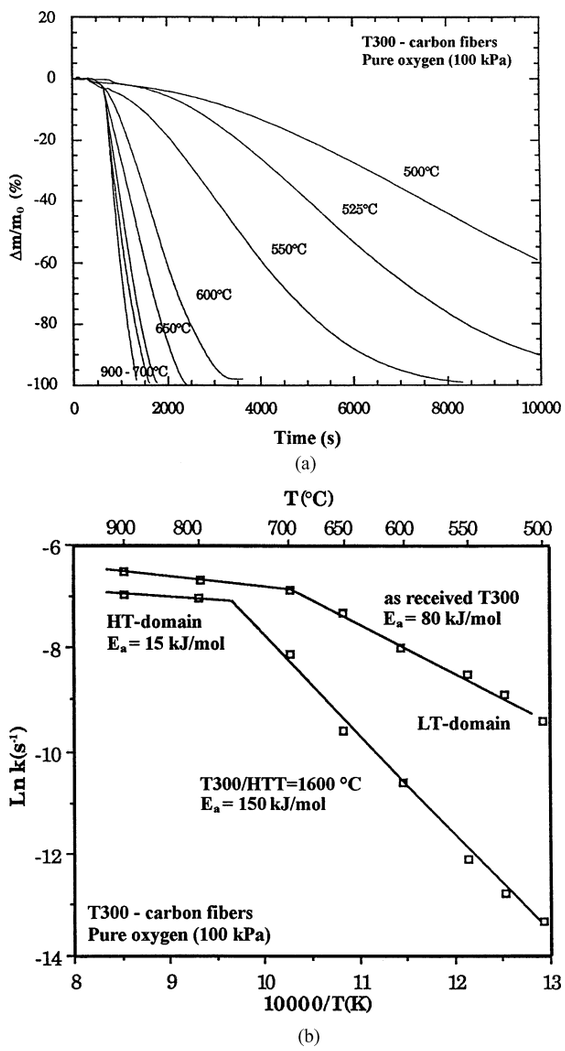

Figure 1 Oxidation kinetics of T300 carbon fiber tows in flowing oxygen (P = 100 kPa; $Q = 10^{-3}$ m^3 per hour): (a) kinetics curves at different temperatures for as-received fibers, (b) Arrhenius plots of the apparent kinetics constants for as-received and heat-treated (HTT = 1600°C) fibers. Redrawn from data of ref. [15, 16].

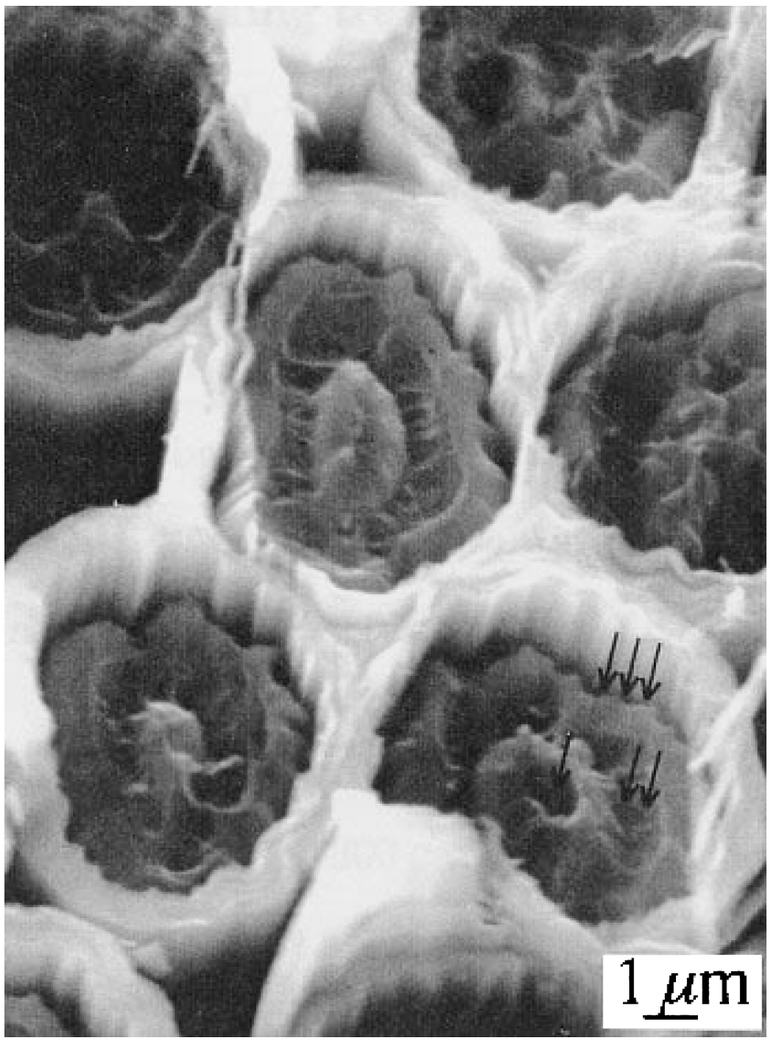

Figure 2 SEM-micrographs of the end of a T300 carbon fiber tows (as-received) infiltrated with a pyrocarbon interphase after a mild oxidation at 550°C in pure oxygen showing the areas of selective oxidation. From ref. [5].

of heteroatoms, including nitrogen and catalytic impurities). The effect of the annealing treatment is related to nanostructural change (and eventually, to a reduction of the heteroatom concentration by volatilization).

Oxidation tests were also performed on T 300 carbon tows in which the individual fibers were coated with a thin layer of pyrocarbon interphase deposited at about 1000°C. As shown in Fig. 2 for a material prepared from as-received fibers, the oxidation rate of the fiber is higher than that of the PyC-coating, which is known to display much better structural organization and hence lower chemical reactivity. Further, the oxidation of the fiber occurs preferentially in specific areas of the cross-section, including the fiber center and the fiber surface, which correlates with the radial microstructural heterogeneity of the fiber [16]. Conversely, in materials prepared with heat treated fibers (HTT = 1600°C), the oxidation rates of the fiber and of the pyrocarbon interphase are now similar but there remains, near the fiber/interphase border, a zone (where heteroatoms are assumed to be concentrated and which displays a high porosity) of high reactivity.

3.2. Oxidation of SiC-based fibers

3.2.1.

The oxidation of Si–C–O and SiC–C fibers, in flowing air or pure oxygen, occurs with the formation of gaseous carbon oxides and a scale of silica (amorphous or crystallized, depending on oxidation conditions), according to the following equations (written for stoichiometric SiC in the passive oxidation regime) [20–25]:

$$SiC_{(s)} + 2O_{2(g)} \rightarrow SiO_{2(s)} + CO_{2(g)} \quad (6)$$

$$SiC_{(s)} + 3/2O_{2(g)} \rightarrow SiO_{2(s,l)} + CO_{(g)} \quad (6')$$

to which, one should add the equations corresponding to the active oxidation of carbon when the fibers contain free carbon :

$$C_{(s)} + O_{2(g)} \rightarrow CO_{2(g)} \quad (7)$$

$$C_{(s)} + 1/2O_{2(g)} \rightarrow CO_{(g)} \quad (7')$$

The silica scale is continuous and protective (passive oxidation regime) since the value of the Δ-factor,

defined as the ratio of the molar volume of silica to that of the fiber (calculated from its composition), is higher than one, namely $\Delta = 1.35$ for the Si—C—O fiber and $\Delta = 1.66$ for the SiC + C fiber (it would still be higher, $\Delta = 2.2$, for the stoichiometric fibers) [8]. For both fibers, the oxidation kinetics curves are parabolic within a given temperature range (as further discussed) and the rate limiting step assumed to be the diffusion of oxygen through the silica scale, by reference to the oxidation of silicon and pure SiC. Hence, they obey the following equations:

$$X^2 = Bt + X_o^2 \quad (8)$$

$$(\Delta m/m_o)^2 = B't + (\Delta m_i/m_o)^2 \quad (8')$$

where B and B' are the so-called parabolic kinetics constants and X_o^2, $(\Delta m_i/m_o)^2$ terms added to take into account the silica eventually present on the fiber surface at $t = 0$. These equations are particular cases of a more general model, referred to as the linear-parabolic model, proposed by Deal and Grove for the oxidation of silicon [26].

3.2.2.

Fig. 3a shows the kinetics curves, recorded under flowing pure oxygen, for the Si—C—O Nicalon fibers and which have been represented as the variations of $(\Delta m/m_o)^2$ as a function of time. As expected, they obey Equation 8′, i.e., they are linear, but only up to 1200°C (at this temperature, a deviation from linearity being observed beyond about 400 minutes). As a matter of fact, this limit corresponds to the onset of the thermal decomposition of the SiC_xO_y amorphous phase present in the fibers and which occurs with an evolution of gaseous species (CO and to a less extent SiO). This additional evolution of CO, if it occurs, would lower the overall weight gain related to the oxidation process. However, the fiber core composition was observed to remain constant during the oxidation test which means that fiber decomposition if it occurs, is limited to near the fiber surface where oxidation concurrently takes place. The silica scale is amorphous at low temperatures but cristobalite has been detected in the scale by XRD at and above 1100°C. Hence, fiber decomposition and/or a change in the scale structure could be responsible for the deviation from linearity observed above 1100°C [4, 20]. An apparent activation energy, $E_a \approx 70$ kJ/mol, has been calculated from the Arrhenius plots of the kinetics parabolic constant B′ (Fig. 3b). This value is much lower than those reported for the oxidation of SiC, namely, ≈200 kJ/mol. On the one hand, this is not totally surprising since the Si—C—O Nicalon fiber is a complex multiphase material, at the nanometer scale, which only contains ≈50 mol% SiC. On the other hand, assuming that the rate limiting step is still the molecular oxygen permeation through the growing silica scale (as for pure SiC), the lower E_a value observed for the fibers suggests that the structure/composition of the scale might be somewhat different. It could be more microporous. It could also contain Si—H or/and Si—OH bonds resulting from interactions between silica and the residual hydrogen (and its oxidation product, H_2O) present in this fiber. Water is known to enhance the oxidation of SiC, even in trace amounts, as further discussed. All these features may cause the diffusion of oxygen through the oxide scale to be easier and lower the apparent activation energy [4, 20].

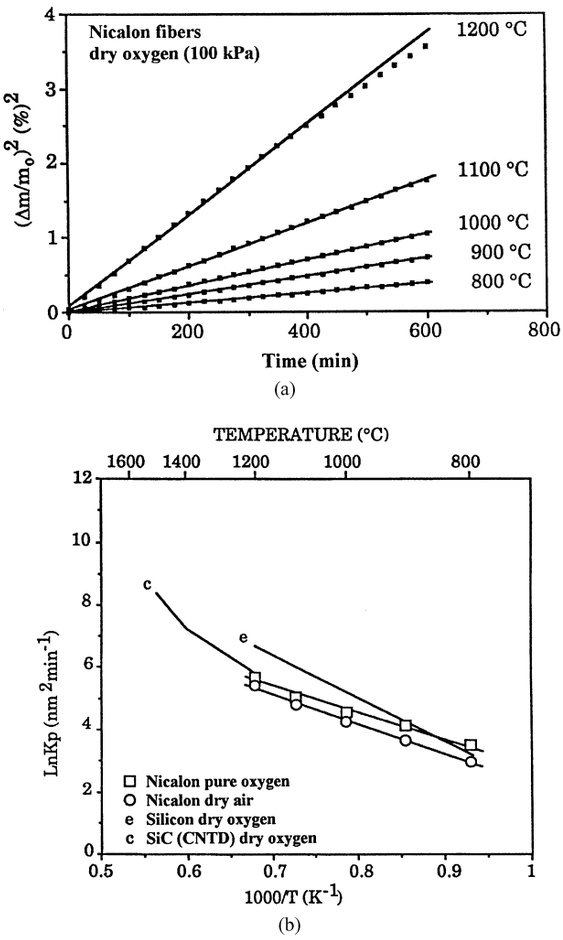

Figure 3 Kinetics of oxidation of the Si—C—O Nicalon (NLM 202/CG) fibers at $P = 100$ kPa: (a) variations of $(\Delta m/m_o)^2$ as a function of time at different temperatures in flowing dry oxygen, (b) thermal variations (Arrhenius plots) of the parabolic rate constant B' (derived from a)) in dry oxygen and dry air (adapted from ref. [4]).

3.2.3.

Oxidation tests were also conducted on the more recent SiC + C (Hi-Nicalon) oxygen free fibers but in a more detailed manner since they are more thermally stable, keep their mechanical properties at higher temperatures and hence are more suitable for the reinforcement of ceramic matrix composites with service temperature higher than 1000°C, compared to their Nicalon counterparts. The tests were performed in oxygen/nitrogen and oxygen/nitrogen/water vapor flowing atmospheres, with different oxygen or/and water vapor partial pressures, in order to assess experimentally full kinetics laws [15].

As shown in Fig. 4a, the variations of the square of the weight gain as a function of time are still linear over the whole studied temperature range (900–1400°C).

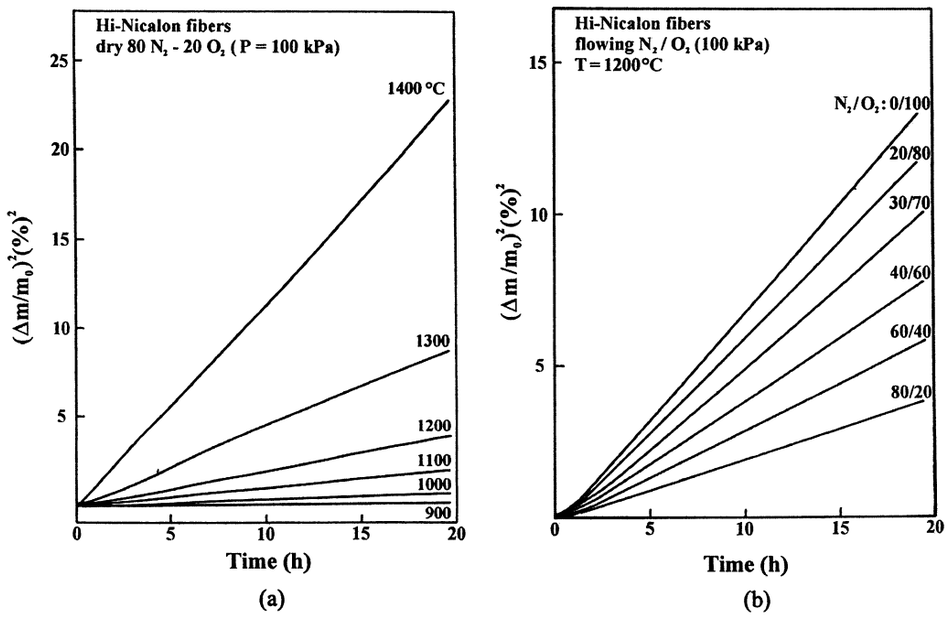

Figure 4 Kinetics of oxidation of SiC + C (Hi-Nicalon) fibers in dry oxygen/nitrogen flowing atmospheres (P = 100 kPa): (a) variations of the square of the weight gain as a function of time at different temperatures in a 80/20 nitrogen/oxygen atmosphere, (b) variations of the square of the weight gain at 1200°C in different nitrogen/oxygen atmospheres (adapted from ref. [15]).

Hence, the oxidation regime is still parabolic (assumed to be rate-controlled by the oxygen-diffusion through the silica scale) and obeys Equation 8′, even above 1200°C. This feature can be correlated with the fact that this fiber is fabricated at higher temperature, does not contain significant amounts of the metastable SiC_xO_y amorphous phase (being almost oxygen-free) and hence does not undergo decomposition in the 1100–1400°C domain, contrary to the behavior of its Nicalon counterpart [8, 22]. The silica scale is amorphous, smooth and dense at 1300°C but it is crystallized as cristobalite and heavily microcracked (after cooling at room temperature, as the result of the α-β phase transformation) for oxidation tests at 1400°C. As shown in Fig. 4b, the oxidation regime is still parabolic when the tests are performed in flowing atmospheres with different oxygen partial pressures: raising the oxygen partial pressure increases the oxidation rate. Furthermore, the variations (in a Ln-Ln scale) of the kinetics constant B' as a function of P_{O_2} are linear, in a first approximation. From these data, an apparent reaction order with respect to oxygen, n = 0.8–0.9, has been calculated (Fig. 5). Finally, an apparent activation energy, E_a = 144 kJ/mol, was derived from the Arrhenius plot of the parabolic rate constant B' as a function of temperature (Fig. 6). It is noteworthy that this value is higher than that previously reported for the Si—C—O Nicalon fibers (E_a = 70 kJ/mol). However, this still low activation energy, compared to those reported for the oxidation of SiC (≈200 kJ/mol) might be correlated with the fact that the fiber also contains a large amount of free carbon (C/Si (at.) ≈1.39).

In a second step, the oxidation tests on SiC + C (Hi-Niclaon) fibers were performed under flowing wet oxygen/nitrogen atmospheres (either at constant P_{O_2} or P_{H_2O} the total pressure being constant and equal to

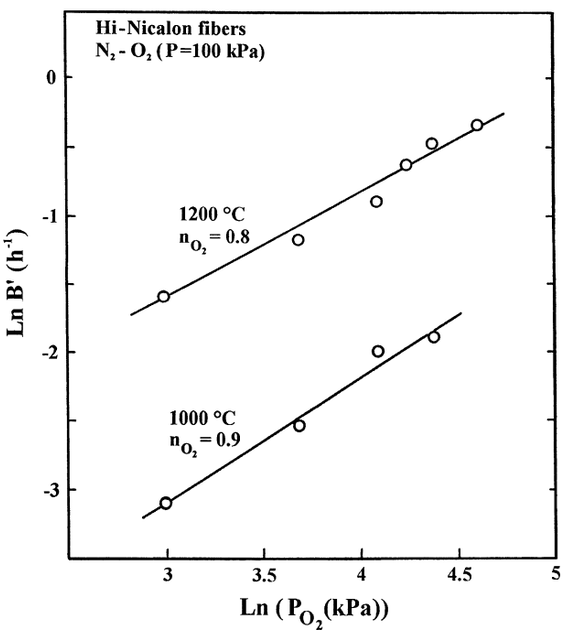

Figure 5 Variations of the oxidation parabolic constant B' as a function of the oxygen partial pressure in flowing oxygen/nitrogen atmospheres (P = 100 kPa), for SiC + C (Hi-Nicalon) fibers (adapted from ref. [15]).

P = 100 kPa), in order to compare the role of the two oxidizing species : oxygen and water vapor. As shown in Fig. 7, the oxidation regime is still parabolic, at least in a first approximation, when water is present in the gas phase, with a dramatic increase in the oxidation rate. As an example, the parabolic rate constant is multiplied by a factor of 20 at 1000°C and 3.5 at 1400°C when the water vapor partial pressure is raised from 0 to 20 kPa (that of oxygen remaining constant and equal to 20 kPa), through the variation of P_{N_2}. Further and as

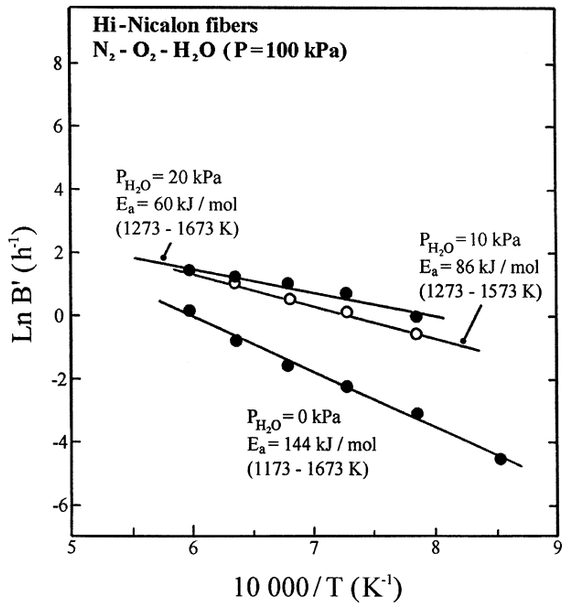

Figure 6 Arrhenius plots of the thermal variations of the oxidation parabolic rate constant B' for SiC + C (Hi-Nicalon) fibers tested in flowing $N_2/O_2/H_2O$ atmospheres (P = 100 kPa and P_{O_2} = 20 kPa) with different P_{H_2O} (adapted from ref. [15]).

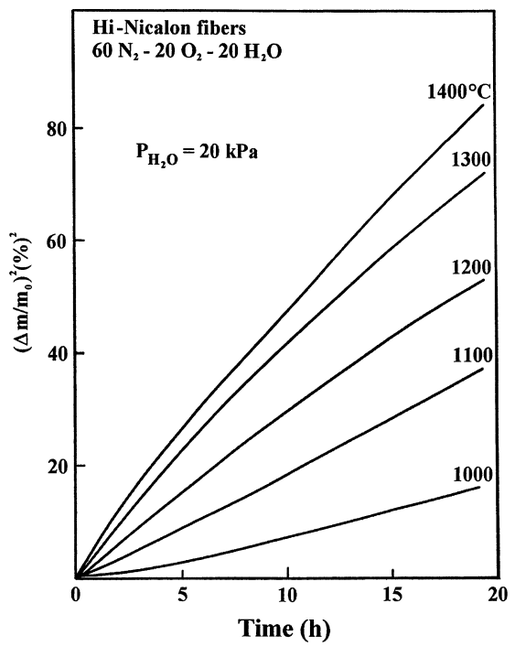

Figure 7 Oxidation kinetics for the SiC + C (Hi-Nicalon) fibers in flowing 60/20/20 nitrogen/oxygen/water vapor atmospheres (P_{total} = 100 kPa) (adapted from ref. [15]).

shown in Fig. 6, the thermal variations of the parabolic rate constant still obey an Arrhenius law with an apparent activation energy of 86 kJ/mol for $P_{H_2O} = 10$ kPa and 60 kJ/mol for $P_{H_2O} = 20$ kPa. Hence, adding water vapor to the oxidizing atmosphere simultaneously increases the oxidation rate and decreases the activation energy to values close to that reported for the molecular diffusion of water in silica ($E_a = 75$ kJ/mol). A similar conclusion has been previously drawn for the oxidation of silicon [26]. This feature suggests that H_2O might be the main oxidizing species in wet oxygen/nitrogen atmosphere, on the one hand, and its molecular diffusion through the silica scale, the rate limiting step. Preliminary complementary oxidation tests conducted at 1200°C in atmospheres containing different oxygen partial pressures (not illustrated here), when combined with the tests at different partial pressures, have shown that the apparent reaction orders with respect to water and oxygen are $n \approx 0.8$ and $n \approx 0.15$, respectively, a result which confirms again the predominant role of water vapor in the oxidation process of the fiber [15]. Finally, the silica scale was observed to mainly be smooth, dense and amorphous at 1200°C and crystallized as cristobalite at 1300°C.

3.3. Oxidation of the SiC-matrix

Oxidation tests were performed in flowing pure dry oxygen (P = 100 kPa; $Q = 10^{-3}m^3$/minute; $H_2O <$ 2 ppm) on the SiC-matrix deposited from MTS + H_2, as depicted in Section 2.2, within the temperature range 900–1500°C. In order to check the influence of the experimental set-up (particularly, that of the TGA alumina tube, which is frequently a source of catalytic sodium impurity), few oxidation tests were also conducted on samples cut in a 300 μm thick single crystal 111 silicon wafer and our results compared to literature data.

As shown in Fig. 8a, the variations of X (the silica scale thickness) as a function of the square root of

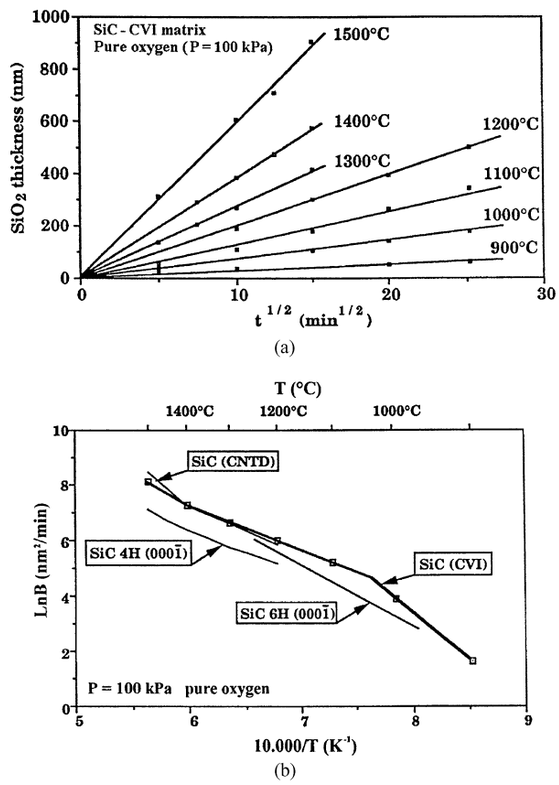

Figure 8 Oxidation kinetics of the CVI SiC-matrix in dry flowing oxygen (P = 100 kPa; $Q = 10^{-3}m^3$ per minute): (a) variations of the silica scale thickness X as a function of the square root of time, (b) Arrhenius plot of the parabolic kinetics constant B: SiC (CVI) [27], SiC (CNTD) [28], 4H-SiC polytype [29], 6H-SiC polytype [31]. Redrawn from ref. [27].

time, are linear and obey Equation 8 (with $X_0^2 \approx 0$). Hence, the oxidation kinetics are again parabolic and rate-controlled by diffusion phenomena (assumed to be the oxygen transfer through the silica scale). The slopes of these straight lines are equal to $B^{1/2}$ and allow the derivation of the parabolic kinetics constant B. Similar results were obtained, as expected, for the silicon wafer and the B-values determined at 1000 and 1200°C were almost identical to those previously reported by Deal and Grove, a feature ruling out a possible contamination by catalytic impurities from the experimental set-up [26, 27]. Interestingly, the silica scale was usually amorphous whatever the temperature, cristobalite being present only for the tests performed at 1500°C, a result which is at variance with those previously mentioned for the SiC-based fibers (containing one or two second phase(s) and heteroatoms) where the formation of cristobalite was observed at much lower temperatures.

Further, the temperature dependence of the parabolic constant obeys the Arrhenius law (Fig. 8b), with an apparent activation energy, $E_a = 128$ kJ/mol, remaining constant in the temperature range 1100–1400°C, a value which is in agreement with those previously published by Tressler and co-workers [28–30]. Beyond 1400°C, there is an increase in the apparent activation energy which has been assigned to a change in the mechanism of oxygen transfer across the silica scale (from oxygen permeation as molecular species to oxygen diffusion as ionic species). Below 1100°C, an increase in apparent activation energy is also observed but its origin still remains uncertain [27]. Finally, the B-parabolic constants for the CVI SiC-matrix are slightly higher than those measured on hexagonal SiC-polytypes [29, 31].

3.4. Oxidation of BN interphases

Preliminary oxidation tests were conducted at one single temperature, i.e., 950°C, under flowing dry reconstituted air ($80N_2$-$20O_2$) at atmospheric pressure (≈100 kPa), on boron nitride deposited from BCl_3-NH_3-H_2 precursor, according to Equation 2. BN was deposited on either Hi-Nicalon fiber tow samples (8 mm in length) or model sintered-SiC flat substrates (all the samples being set *horizontally* in the TGA-apparatus).

In dry air, the oxidation is assumed to proceed according to the following overall equation:

$$2BN_{(s)} + 3/2O_{2(g)} \rightarrow B_2O_{3(s,l)} + N_{2(g)} \qquad (9)$$

corresponding to a Δ-factor, defined as the ratio of the molar volume of B_2O_3 to that of 2BN, equal to 2.1. As a result, the oxide is expected to form a covering scale and the oxidation regime to be passive, as previously described for the oxidation of SiC-based materials. However, $B_2O_3$is liquid above ≈410°C. Its viscosity decreasing as temperature is raised, it tends to flow and to form droplets, thus modifying the nominal oxide film thickness. Further, B_2O_3 undergoes vaporization at sufficiently high temperatures, namely beyond 1000–1100°C in dry air, but at much lower temperatures if the atmosphere contains water (even in trace amounts), according to the main following overall equation [32, 33]:

$$B_2O_{3(l)} + H_2O_{(g)} \rightarrow 2HBO_{2(g)} \quad \text{at } T \geq 1000^\circ C \qquad (10)$$

$$3/2B_2O_{3(l)} + 3/2H_2O_{(g)} \rightarrow (HBO_2)_{3(g)} \qquad (10')$$

$$1/2B_2O_{3(l)} + 3/2H_2O_{(g)} \rightarrow H_3BO_{3(g)} \quad \text{at } T < 1000^\circ C \qquad (10'')$$

Hence, it is often considered more appropriate to study BN-oxidation kinetics from the variations versus time of the amount of BN consumed by oxidation than from those of the weight of B_2O_3 on the substrate [34]. Finally, the oxidation of BN (in its hexagonal (ordered) or turbostratic (disordered) forms) is *highly anisotropic*, as that of graphitic carbons, the oxidation rate being much higher at the layer edges (where are mainly located the reaction sites) than in a direction perpendicular to the layers. For all these reasons, the oxidation kinetics of BN are more complex than those previously reported for SiC-based materials: they often are linear (rate control by surface reaction), rarely parabolic (rate control by oxygen diffusion through the oxide scale), or a combination of both and strongly depending on the crystallinity and microstructure of BN.

The oxidation curves, as derived from TGA experiments, for BN deposited on Hi-Nicalon fiber tows with different α-ratios (with $\alpha = NH_3/BCl_3$ and $\alpha_3 > \alpha_2 > \alpha_1 \geq 1$) are presented in Fig. 9. These curves can tentatively be analyzed as follows. Firstly, there is an *induction* period of about 1 h during which some BN is consumed (Fig. 9a) but with almost no condensed B_2O_3 formation (Fig. 9b). This feature could be related to the progressive activation of the reaction sites (layer edges). As a matter of fact, BN deposited by CVD/CVI at low temperatures and further heat treated is strongly textured (the BN layers being parallel to the deposit surface) and hence poorly reactive (reaction sites being initially limited to near fiber ends). Secondly, the oxidation rate strongly depends on α and hence on the state of crystallization of BN after the HTT (crystallinity being higher for $\alpha = \alpha_3$ than for $\alpha = \alpha_1$) [6]. Finally, after the induction period, the oxidation curves $X^2\,(B_2O_3) = f(t)$ seem to be linear (Fig. 9b), suggesting a parabolic regime.

A similar conclusion was drawn from oxidation tests conducted on a free standing commercial boron nitride (from Advanced Ceramics, USA), ≈2 mm in thickness, deposited from the same precursor but at a temperature of ≈2000°C. This material is a highly textured, true 3D-ordered hex-BN with the layers parallel to the surface. In the oxidation samples cut from this material, the layer edges bearing the reaction sites are apparent on the *lateral faces* which represent a given percentage δ of the total sample surface. This factor decreases as the sample lateral size (ℓL) increases (the thickness h being constant), as shown in Fig. 10a. It is worthy of note that: (i) the kinetics curves $X^2\,(B_2O_3) = f(t)$ are linear (with no induction period since here the reaction sites are initially numerous), suggesting a parabolic oxidation regime, as mentioned above for the fibrous samples and

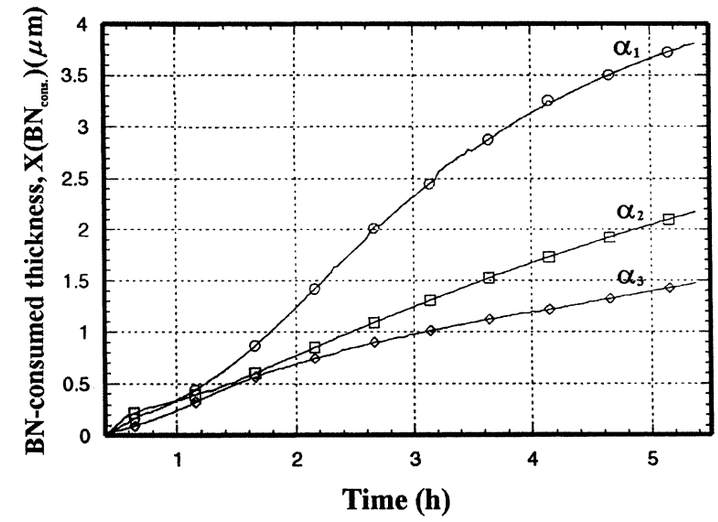

(a)

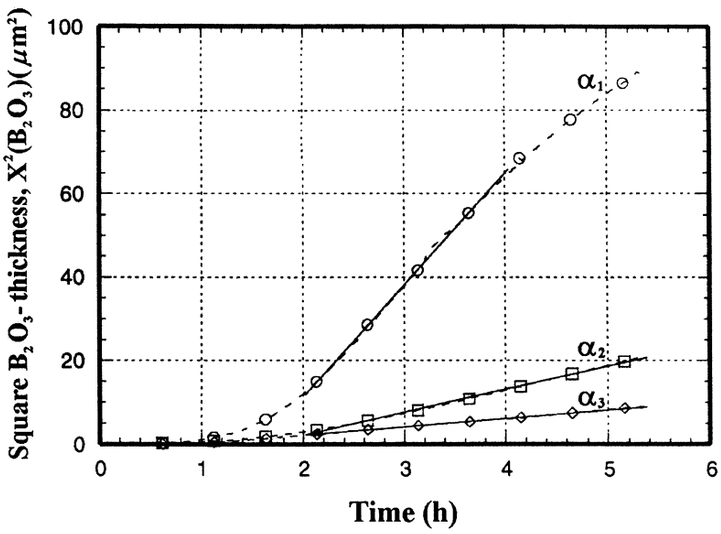

(b)

Figure 9 Oxidation kinetics, under dry reconstituted air at 950°C and $P \approx 100$ kPa, of heat-treated Hi-Nicalon fiber tow coated with a BN-interphase deposited with different $\alpha = NH_3/BCl_3$ ratios: (a) variations of the BN-thickness consumed as a function of time, (b) variations of the square of the B_2O_3-thickness as a function of time. The kinetics curves were derived from TGA-data (redrawn from ref. [6]).

(ii) the oxidation rate increases as the δ-value (i.e., the number of reaction sites) increases (Fig. 10b).

Conversely, the oxidation tests performed directly on BN deposited at low temperature on sintered SiC-pellets, further heat-treated as previously depicted and which have received *no machining*, yield different data, as shown in Fig. 11. Firstly, there is a long induction period, at least for the best crystallized materials ($\alpha = \alpha_2$ or α_3) since the textured BN-deposit is *continuous* all over the pellet surface with almost no layer edges (reaction sites) apparent at the deposit surface. Hence, reaction sites have to be created (by oxidation etching) and activated. Secondly, after this activation period, the oxidation curves are linear and not parabolic suggesting that the oxidation kinetics are depending on surface reactions and deposit microstructure.

These preliminary data clearly show that the oxidation of BN-interphases deposited at low temperatures (a requirement in the CVI-process for fiber-preforms) from BCl_3-NH_3-H_2 precursor and which cannot be heat-treated at very high temperatures (owing to the limited thermal stability of Hi-Nicalon fibers), obey complex kinetics laws which depend on the structure and microtexture of the BN-deposit.

3.5. Oxidation of SiC-matrix model or real composites

When a SiC-matrix composite, reinforced with carbon or SiC-based fibers precoated with a PyC or BN interphase, is exposed to an oxidizing atmosphere, both active and passive oxidation phenomena occur simultaneously which result either in a degradation or a preservation of the composite properties, depending on the oxidation conditions and composite microstructure [4, 5]. This is illustrated in the two following examples for model or real composites.

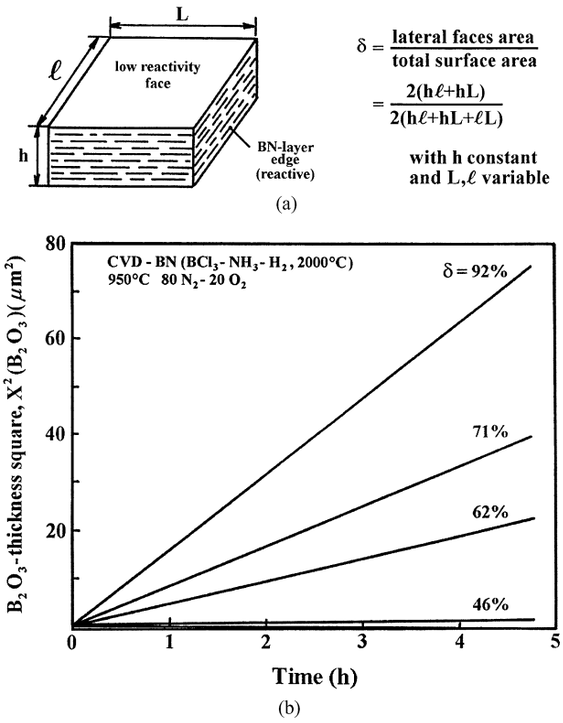

Figure 10 Oxidation kinetics of self standing hex-BN, deposited at 2000°C from BCl_3-NH_3-H_2 gaseous precursor, under flowing reconstituted dry air at 950°C and $P \approx 100$ kPa: (a) geometry of the samples and definition of the δ-factor, (b) oxidation curves, derived from TGA-data, for different δ-values.

3.5.1. 1D-SiC (Nicalon)/PyC/SiC model composites

The model composites considered here were fabricated by the CVI-process, the fibers (Si—C—O Nicalon fibers) being unidirectionally oriented. They comprised either a thin (0.1 μm) or a thick (1 μm) pyrocarbon interphase deposited from methane as well as a relatively thick SiC-overcoating used to seal the residual porosity.

The two faces of the parallelepiped shaped oxidation samples perpendicular to the fiber direction were machined to provide controlled access of oxygen to the inside of the material. TGA-oxidation tests were conducted under flowing dry oxygen (P ≈100 kPa) at a temperature ranging from 700 to 1400°C. Representative oxidation curves are shown in Fig. 12 (for the composites with the thin PyC-interphase) and can be analyzed, as follows, on the basis of three domains [4, 36]. There is first a relatively sharp weight loss (domain I) corresponding to the active oxidation of the carbon interphase with formation of carbon oxides (CO_2 and/or CO). It is followed, after a transition period (domain II), by a progressive weight gain (domain III) related to the passive oxidation of the SiC-matrix and seal-coating as well as the Si—C—O fibers with formation of silica scales and carbon oxides, according to Equations 6 to 7′. At low temperatures, the extent of domain I is large (at 700°C both domains II and III are even not observed at all) since the oxidation rates of the SiC-based constituents are low whereas that of the PyC-interphase is already relatively high. As temperature is raised, the domain I extent becomes narrower and the weight loss lower and lower. Further, the transition domain II is shifted to shorter times and the weight gain (domain III) more and more significant.

All the features of the oxidation TGA-curves of the model composites can be interpreted on the basis of a competition between the oxidation reactions and the diffusion of oxygen along the annular pore which is formed around each fiber by the oxidation of the PyC-interphase (Fig. 13). Oxygen has to diffuse along that pore to react with the carbon interphase. During this diffusion, it may also react passively with the inner and outer pore walls to form silica layers. At low temperatures, the rates of formation of the silica scales on the pore walls are slow and the active oxidation of the PyC-interphase proceeds in-depth with the result that the interphase can be almost totally consumed with an important weight loss (700°C curve in Fig. 12). By contrast at high temperatures, silica is formed rapidly and

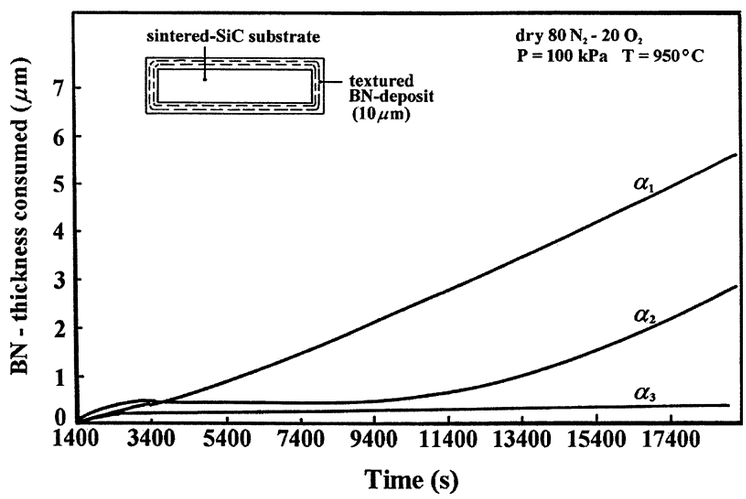

Figure 11 Oxidation kinetics, at 950°C under flowing dry reconstituted air ($P \approx 100$ kPa), of BN-films deposited at low temperature from BCl_3-NH_3-H_2 and further heat-treated. The inset shows, in cross-section, the continuity of the BN-deposit (redrawn from ref. [6]).

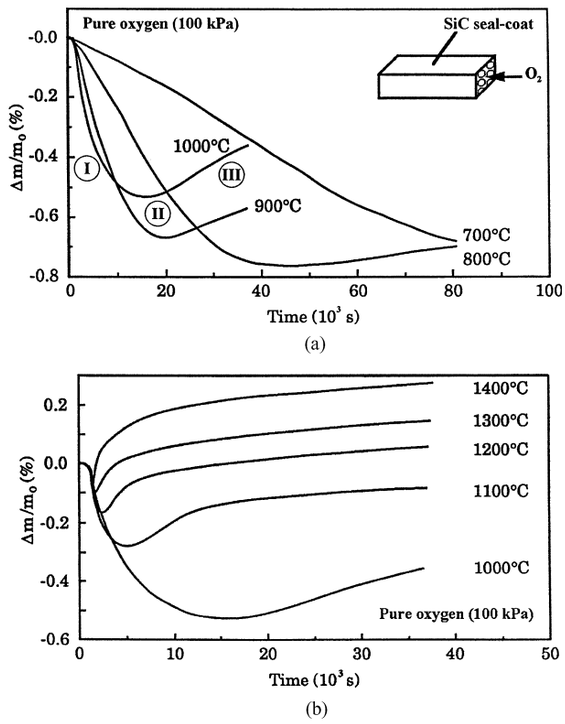

Figure 12 Oxidation TGA-curves for SiC-coated 1D-Nicalon/PyC/SiC composites fabricated by CVI, in dry flowing oxygen ($P \approx 100$ kPa) at different temperatures: (a) 700 $< T <$ 1000°C, (b) 1000 $< T <$ 1400°C, adapted from ref. [4] and [36].

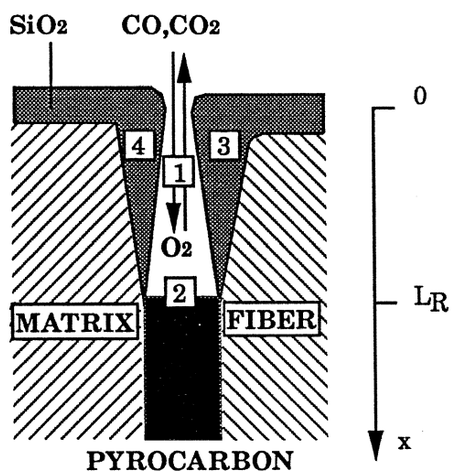

Figure 13 Elementary phenomena occurring during the oxidation of 1D-SiC/C/SiC model composites: (1) diffusion of reactant (O_2) and products (CO/CO_2) along annular pore, (2) active oxidation of PyC-interphase, (3) (4) formation of silica scales (passive regime) on pore walls, according to ref. [4] and [36].

can seal the pores entrances in a short time. Consequently, little PyC interphase is consumed, weight loss is limited (domain I) and the weight gain (domain III) is significant (1400°C curve in Fig. 12).

The composite architecture and the oxygen transfer by diffusion along the annular pores being unidirectional, the oxidation phenomena depicted above have been modelled on the basis of the classical diffusion equations, utilizing the kinetics laws discussed previously in Sections 3.1, 3.2 and 3.3 (see Ref. [37] for

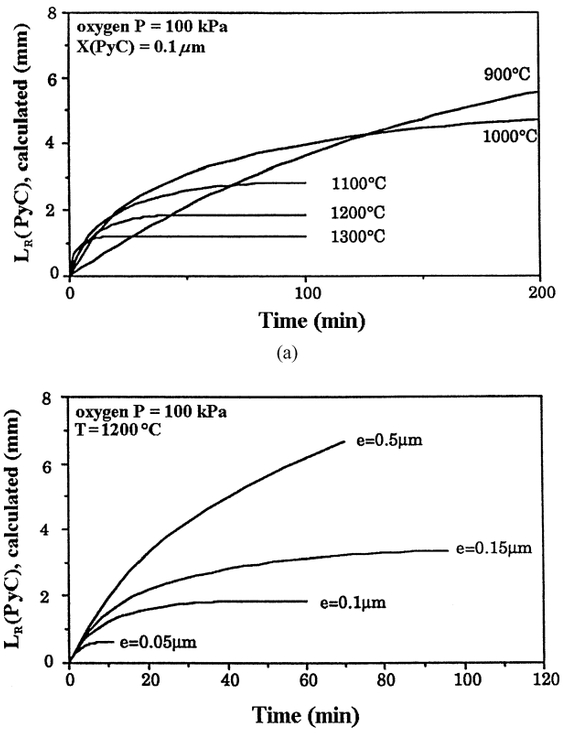

Figure 14 Calculated length, L_r, of PyC-interphase consumed by oxidation in pure oxygen for 1D-Nicalon/C/SiC composites fabricated by CVI, as a function of time: (a) at different temperatures for a 0.1 μm thick interphase, (b) for different interphase thicknesses at 1200°C, adapted from ref. [4] and [37].

details). The calculated TGA-curves were observed to be in good agreement with the experimental data. Further, the model has been used to predict the influence of a given parameter on the oxidation of the composite. As an example, Fig. 14 shows the effect of temperature and interphase thickness on the length L_r of PyC-interphase consumed by oxidation from the pore entrance. It clearly appears that the material has a much better behavior in oxygen, i.e., the PyC-interphase vaporization is limited to near the external machined surface, at high temperature and when the interphase is thin, the materials being referred to as *self-healing* under such conditions [37].

3.5.2. 2D-C/PyC/SiC real composites

SiC-matrix 2D-composites have been fabricated by CVI, from a stack of carbon fiber fabrics (T 300) coated with a pyrocarbon interphase. The samples for the oxidation tests were cut in the composite, seal-coated with a relatively thick layer of SiC by CVI (to seal the residual porosity) and finally heat-treated at 1600°C (to stabilize the microstructure). The samples were heavily microcracked (in both the SiC-matrix and seal-coating), in the as-fabricated state, as the result of thermal expansion mismatch: the microcraks being widely open at room temperature and very narrow at high temperatures. The oxidation TGA-tests were conducted in flowing dry oxygen or air ($P \approx 100$ kPa) [5, 38, 39].

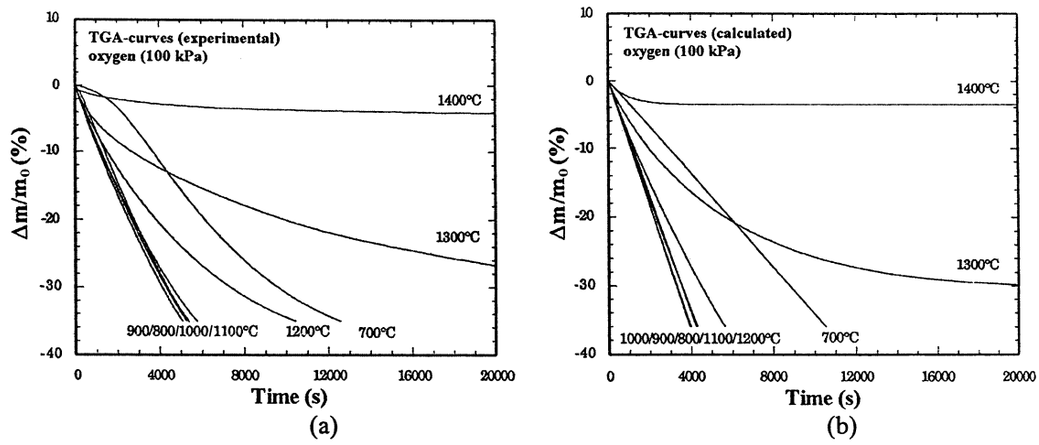

Figure 15 Oxidation kinetics of a 2D-C (T 300)/PyC/SiC composite in flowing dry oxygen ($P \approx 100$ kPa) as assessed: (a) from TGA-experiments and (b) by modelling. Adapted from ref. [5] and [39].

Representative oxidation curves are shown in Fig. 15a for $700 \leq T \leq 1400°C$ and flowing oxygen. These curves can be classified into three families. At low ($T < 800°C$) and medium ($800 < T < 1100°C$) temperatures, a very important weight loss occurs, tentatively assigned to the active oxidation (Equations 7 and 7′) of the PyC-coated carbon fibers by oxygen diffusing in-depth along the microcracks. The oxidation rate increases as temperature is raised (see Section 3.1). At high temperatures ($1100 < T < 1400°C$), the overall weight loss progressively decreases to become almost nil at 1400°C.

The oxidation of the composite has been modelled on the basis of (i) the oxygen diffusion along the microcracks of the SiC-matrix and seal-coating (Fig. 16) taking into account the variations of the microcrack opening as a function of temperature and (ii) the chemical reactions between oxygen and both the SiC microcrack wall and carbon from the interphase and fibers, utilizing the kinetics laws discussed in Sections 3.1 to 3.3. It was further assumed that oxygen arriving at the SiC-microcrack tip was totally consumed by reaction with carbon (see ref. [39] for details). The model was used to calculate the TGA-curves and to study the influence of different parameters on the oxidation of the composite.

As shown in Fig. 15 there is a fair agreement between the calculated and experimental TGA-curves. Since the

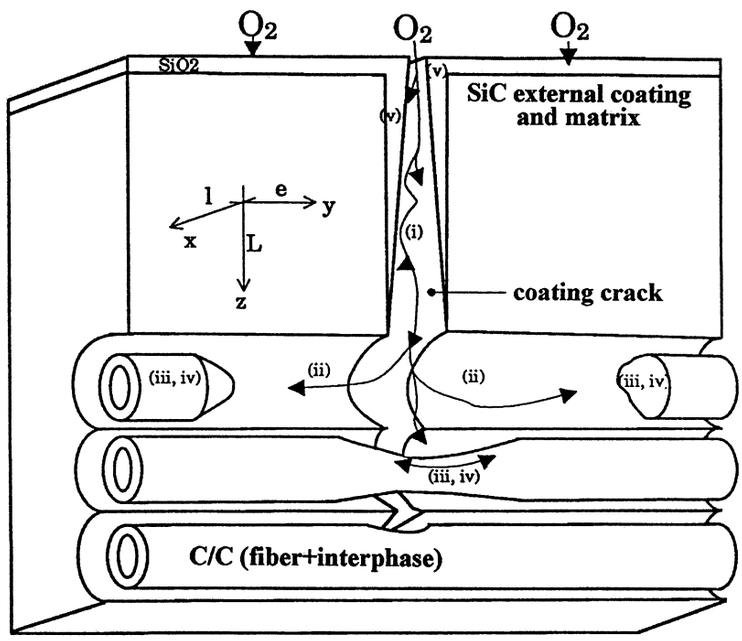

e: crack width; l: crack length; L: crack depth.

Figure 16 Phenomena occurring during the oxidation of 2D-C (T 300)/PyC/SiC composites: (i) diffusion along the SiC-microcracks, (ii) diffusion in the pore created by oxidation of carbon phases, (iii) diffusion of oxygen at carbon surface to reaction sites, (iv) surface reaction, (v) growth of silica on SiC-microcrack wall. Adapted from ref. [5] and [39].

contribution of the different phenomena (Fig. 16) was taken into account in the model, it now appears that at low temperatures ($T < 800°C$), the oxidation kinetics are controlled by the in-depth, carbon /oxygen reaction: the SiC-microcracks are widely open, little oxygen reacts with the SiC-microcrack wall since the oxygen/SiC reaction kinetics are slow. Further, since the reactivity of the carbon phases is still low compared to the rate of oxygen diffusion in the microcracks, the carbon reinforcement is uniformly degraded in the whole sample. At intermediate temperatures ($800 < T < 1100°C$), the microcracks are narrower and diffusion of the gaseous species in the microcracks becomes the rate-controlling step. Consequently, the degradation of the carbon reinforcement is no longer uniform: it is more significant near the surface than in the bulk. Finally, at high temperatures ($1100 < T < 1400°C$), the microcracks are now very narrow and the oxygen flux along them is limited. Further, since the kinetics of the SiC/oxygen reaction are now fast, the microcracks are rapidly sealed by silica (self-healing character). Consequently, the degradation of the carbon reinforcement is limited to near the composite surface. Further, the formation of silica in the microcrack network and on the external surface of the material (SiC-seal-coating) significantly reduces the overall weight loss.

3.5.3. Remarks

Some conclusions reported above have been used to improve the oxidation resistance of SiC-matrix composites (assuming that one remains in the passive oxidation regime of SiC). Firstly, there is an advantage in developing the concept of *self-healing* materials, through the introduction of constituents, such as boron -or silicon-bearing compounds (BN, B_4C, SiC, SiB_6 or ternary phases) forming fluid oxides (B_2O_3, SiO_2 or B_2O_3-SiO_2) in oxidizing atmosphere and sealing microcracks as they form under load. Further, the healing process is easier when the cracks (or pores) are narrow rather than broad (see Fig. 14b). Secondly, SiC matrix composites display better behavior in oxidizing atmospheres at high temperature due to the formation of silica.

On the basis of the above remarks, several material concepts have been successfully introduced. In *multilayered interphases*, the mechanical fuse (PyC or BN) instead of being used as a single relatively thick layer (0.1 to 0.3 μm) is subdivided into extremely thin layers (few nm to few 10 nm), a design which renders much easier the crack healing phenomena [2, 40]. This concept has been further extended to the matrix itself, replacing the homogeneous SiC-matrix by a *multilayered matrix* combining layers of materials deflecting cracks with layers forming fluid oxides in oxidizing atmospheres [41], as well as to the external coating. Finally, the use of more-thermally stable SiC-fibers (such as the stoichiometric SiC-fibers) combined with BN-interphases deposited at low temperature, would permit heat-treatment at high temperatures, improving thus the crystallinity and oxidation resistance (particularly in wet atmospheres) of this kind of interphase whose design is not yet fully achieved.

4. Conclusion

On the basis of the data reported and discussed in Section 3, the following conclusions can be tentatively drawn:

1. The oxidation kinetics of SiC fibers and matrix are parabolic and assumed to be rate-controlled by the diffusion of gaseous species (oxygen) in the silica scale. However, the apparent activation energy for the fibers is lower than for pure SiC, possibly due to secondary phases and impurities. Finally, the apparent reaction order with respect to oxygen partial pressure is close to one.
2. The oxidation of SiC-based fibers is accelerated in wet atmospheres. Oxidation kinetics are still parabolic but with a much lower activation energy. Water, rather than oxygen, could be the main oxidizing agent.
3. The oxidation of carbon fibers and interphases is rate-controlled by diffusion at high temperatures and by a combined diffusion/chemical reaction mechanism at low temperatures. Heat treating the fibers at 1600°C lowers their oxidation rate and both increases the activation energy and the role of surface reactions. The oxidation rate of the PyC-interphase is lower than that of the as-received fibers but similar when the fibers are heat-treated at 1600°C.
4. The oxidation of boron nitride deposited by CVD is strongly anisotropic: it is easy at layers edges where the active reaction sites are mainly located and difficult in a direction perpendicular to the layers. It is parabolic when the active sites are numerous. Conversely, it requires an induction period when it is not the case. The oxidation rate of BN-interphase deposited by CVD depends on the composition, structure and texture of the deposit and hence it can be significantly reduced by heat-treatment. Increasing temperature or/and adding water to the atmosphere favors the vaporization of B_2O_3-scale.
5. The oxidation of SiC-matrix composites involves both the diffusion of gaseous species in the material porosity and heterogeneous oxidation reactions. At low temperatures, the oxidation is an in-depth phenomenon which consumes the PyC-interphase and carbon fibers since the growth kinetics of the protective silica scale are too slow. At high temperatures, it tends to be limited to near the composite surface, silica (whose formation is now fast) healing the cracks and porosity of the material and preventing thus the in-depth oxidation of the carbon phases.
6. Finally, the oxidation of SiC matrix composites has been modelled utilizing the kinetics laws established for the elementary constituents. The models are interesting tools for studying the influence of different parameters on the oxidation kinetics and for designing composites with improved oxidation resistance.

References

1. R. NASLAIN, in "The Art of Ceramics: The Blend of Art and Science in Technology," edited by N. Claussen, Discussions of the Academy of Ceramics, Forum 2000 (Techna, Faenza, 2001) p. 13.
2. *Idem.*, *Composites Part A* **29A** (1998) 1145.
3. *Idem.*, *Comp. Sci. Techn.* **64** (2004) 155.

4. L. FILIPUZZI, "Oxidation of SiC/SiC Composites and Their Constituents: Experimental Approach, Modelling and Effect on the Mechanical Behavior," PhD Thesis no 593, Univ. Bordeaux 1, March 29, 1991.
5. F. LAMOUROUX, "Behavior of 2D C/SiC Composites in an Oxidizing Environment," PhD Thesis no 860, Univ. Bordeaux 1, Dec. 8, 1992.
6. S. LE GALLET, "The Multilayered Boron Nitride Interphase in SiC/SiC Thermostructural Composites," PhD Thesis no 2476, Univ. Bordeaux 1, Dec. 19, 2001.
7. R. NASLAIN, A. GUETTE, F. LAMOUROUX, G. CAMUS, C. LABRUGERE, L. FILIPUZZI and J. THEBAULT, in Proc. 10th Intern. Conf. Composite Mater. (ICCM-10), edited by A. Poursartip and K. Street (Woodhead Publ., Ltd., Abington/Cambridge, 1995) vol. 4, p. 759.
8. R. NASLAIN, in "Advanced Inorganic Fibers," edited by F. T. Wallenberger (Kluwer Academic Publishers, Boston, 2000) p. 265.
9. S.-M. DONG, G. CHOLLON, C. LABRUGERE, M. LAHAYE, A. GUETTE, J. L. BRUNEEL, M. COUZI, R. NASLAIN and D.-L. JIANG, *J. Mater. Sci.* **36**(10) (2001) 2371.
10. R. NASLAIN and F. LANGLAIS, "Mater. Sci. Res." (Plenum Press, New York, 1986), vol. 20, p. 145.
11. F. REBILLAT, "Properties of the Interfaces and Interphases in Ceramic Matrix Composites," PhD Thesis no 1397, Univ. Bordeaux 1, Jan. 24, 1996.
12. R. NASLAIN, O. DUGNE, A. GUETTE, J. SEVELY, C. ROBIN-BROSSE, J. P. ROCHER and J. COTTERET, *J. Amer. Ceram. Soc.* **74** (1991) 2482.
13. F. LOUMAGNE, F. LANGLAIS and R. NASLAIN, *J. Cryst. Growth* **155** (1995) 198.
14. R. NASLAIN, J. LAMON, R. PAILLER, X. BOURRAT, A. GUETTE and F. LANGLAIS, *Comp. Part A: Appl. Sci.* **30**(4) (1999) 537.
15. C. LOUCHET-POUILLERIE, P. DISS, D. BARRIERE, J. C. CAVALIER, F. REBILLAT, A. GUETTE and R. NASLAIN, *Extended Abstract*, GFC-Meeting, 20–27 March 2001, Saint-Etienne, France (in French).
16. F. LAMOUROUX, X. BOURRAT, R. NASLAIN and J. SEVELY, *Carbon* **31** (1993) 1273.
17. H. MARSH and K. KUO, in "Introduction to Carbon Science," edited by H. Marsh (Butterworths, London, 1989) p. 107.
18. M. K. ISMAIL, *Carbon* **29**(6) (1991) 777.
19. Y. T. ZHU, S. T. TAYLOR, M. G. STOUT, D. P. BUTT and T.C. LOWE, *J. Amer. Ceram. Soc.* **81**(31) (1998) 655.
20. L. FILIPUZZI and R. NASLAIN, in *Mater. Sci. Monographs* **68** "Advanced Structural Inorganic Composites," edited by P. Vincenzini (Elsevier, Amsterdam, 1991) p. 35.
21. T. SHIMOO, Y. MORISADA and K. OKAMURA, *J. Amer. Ceram. Soc.* **83**(12) (2000) 3049.
22. G. CHOLLON, C. LAPORTE, R. PAILLER, R. NASLAIN, F. LAANANI, M. MONTHIOUX and P. OLRY, *J. Mater. Sci.* **32** (1997) 327.
23. T. SHIMOO, F. TOYODA and K. OKAMURA, *ibid.* **35** (2000) 3301.
24. T. SHIMOO, Y. MORISADA and K. OKAMURA, *ibid.* **37** (2002) 4361.
25. T. SHIMOO, H. TAKEUCHI, M. TAKEDA and K. OKAMURA, *J. Ceram. Soc. Jpn.* **108**(12) (2000) 1096 (in Japanese).
26. B. E. DEAL and A. S. GROVE, *J. Appl. Phys.* **36**(12) (1965) 3770.
27. L. FILIPUZZI, R. NASLAIN and C. JAUSSAUD, *J. Mater. Sci.* **17** (1992) 3330.
28. J. A. COSTELLO and R. E. TRESSLER, *J. Amer. Ceram. Soc.* **69**(9) (1986) 674.
29. Z. ZHENG, R. E. TRESSLER and K. E. SPEAR, *J. Electrochem. Soc.* **137**(3) (1990) 854.
30. *Idem., ibid.* **137**(9) (1990) 2812.
31. R. C. A. HARRIS, *J. Amer. Ceram. Soc.* **58**(1/2) (1975) 7.
32. N. JACOBSON, S. FARMER, A. MOORE and H. SAYIR, *ibid.* **82**(2) (1999) 393.
33. N. S. JACOBSON, G. N. MORSCHER, D. R. BRYANT and R. E. TRESSLER, *ibid.* **82**(6) (1999) 1473.
34. K. ODA and T. YOSHIO, *J. Mater. Sci.* **28** (1993) 6562.
35. F. REBILLAT, S. LE GALLET, A. GUETTE, X. BOURRAT and R. NASLAIN, in "High Temperature Ceramic Matrix Composites," edited by W. Krenkel *et al.* (Wiley-VCH, Weinheim, 2001) p. 193.
36. L. FILIPUZZI, G. CAMUS, R. NASLAIN and J. THEBAULT, *J. Amer. Ceram. Soc.* **77**(2) (1994) 459.
37. L. FILIPUZZI and R. NASLAIN, *ibid.* **77**(2) (1994) 467.
38. F. LAMOUROUX, G. CAMUS, R. NASLAIN and J. THEBAULT, *ibid.* **77**(8) (1994) 2049.
39. F. LAMOUROUX, R. NASLAIN and J. M. JOUIN, *ibid.* **77**(8) (1994) 2058.
40. S. BERTRAND, O. BOISRON, R. PAILLER, J. LAMON and R. NASLAIN, *Key Engng. Mater.* **164–165** (1999) 357.
41. F. LAMOUROUX, S. BERTRAND, R. PAILLER, R. NASLAIN and M. CATALDI, *Comp. Sci. Techn.* **59** (1999) 1073.

Received 25 February
and accepted 31 August 2004